Real-time and short-term predictions of spring phenology in North America from VIIRS data

Lingling Liu[1*], Xiaoyang Zhang[1,2], Yunyue Yu[3], and Wei Guo[4]

1. Geospatial Sciences Center of Excellence (GSCE), South Dakota State University, 1021 Medary Ave, Brookings, SD, 57007, USA
2. Department of Geography, South Dakota State University, Brookings, SD 57007, USA
3. NOAA/NESDIS/STAR, 5200 Auth Rd, Camp Springs, MD 20746, USA.
4. I. M. Systems Group at NOAA/NESDIS/STAR, 5200 Auth Rd, Camp Springs, MD 20746, USA.

*Corresponding author: Lingling Liu
Tel.: +1 605 688 4921
Fax: +1 605 688 5227
E-mail: Lingling.Liu@sdstate.edu

Abstract: Real-time prediction of vegetation phenology is critical for assisting crop monitoring, natural resource management, and land modeling in weather prediction systems. However, due to the lack of timely available satellite datasets and the inherent noise in time series, little attention has been paid to real-time and short-term predictions of vegetation phenology. The successful launch of the Visible Infrared Imaging Radiometer Suite (VIIRS) instrument onboard operational Suomi National Polar-orbiting Partnership (Suomi NPP) satellite makes this research possible because it can provide land surface observations in a timely fashion. This study introduces an operational system that provides real-time and short-term predictions of vegetation phenology. Specifically, the system integrates timely available VIIRS observations and the climatology (expectation and standard deviation) of vegetation phenology from long-term MODIS data to simulate a set of potential temporal trajectories of greenness development at a given time for each pixel. These potential trajectories are then applied to identify spring green leaf development in real time, predict the occurrence of greenup onset, mid greenup phase and maturity onset, and analyze the uncertainty of the prediction across a variety of ecosystems in North America. The accuracy of real-time and short-term predictions was evaluated by comparing with standard VIIRS detections and near-surface PhenoCam observations in both 2014 and 2015 across North America. The results showed that the real-time prediction of spring phenological metrics from VIIRS were all significantly correlated with those derived from PhenoCam datasets ($R^2 > 0.96$, $P<0.01$) and closely comparable to the standard VIIRS detections with a mean absolute difference of less than 10 days, 5 days and 5 days in greenup onset, mid greenup phase and maturity onset, respectively. The mean absolute difference in the northern region for all three events was relatively smaller than that in the southern region. These findings demonstrate the capability of VIIRS observations to effectively predict temporal dynamics of vegetation phenology in real time at a continental scale.

Keywords: spring phenology; VIIRS; real-time and short-term prediction; climatology of vegetation phenology

1. Introduction

The timing of plant phenology, the recurrence of life cycle events, is important for understanding the response of ecosystems to climate change, the exchange of energy, carbon, and water vapor between the biosphere and atmosphere, and habitat and biodiversity (Cleland et al. 2007; Ganguly et al. 2010; Menzel et al. 2006). It can be monitored by several approaches including direct field observations, modelling, near-surface digital camera imaging and satellite remote sensing (Ault et al. 2015; Liu et al. 2015; Menzel et al. 2006; Richardson et al. 2011; Schwartz et al. 2013; Zhang et al. 2014). Phenology datasets collected from field observations and near-surface digital camera (PhenoCam) at specific sites only focused on individual plants or communities in a small region. In contrast, phenology derived from satellite remote sensing, which is termed land surface phenology (LSP) (Henebry and de Beurs 2013), is the only way to quantify seasonal dynamics of vegetation properties over a large scale (Ganguly et al. 2010; Moulin et al. 1997; Zhang et al. 2006).

To date, studies have been focusing on estimating land surface phenology using historical satellite datasets from AVHRR (Advanced Very High Resolution Radiometer), MODIS (Moderate Resolution Imaging Spectroradiometer) and Landsat during the past several decades (Fisher and Mustard 2007; Reed et al. 1994; Stöckli and Vidale 2004; Zhang et al. 2014; Zhang et al. 2003). The phenological metrics for a year are commonly detected from a time series of two years that consist of preceding half year, a given year, and following half year (Ganguly et al. 2010; Zhang et al. 2006) because of the noises and frequent cloud contaminations in the time series of satellite observations, which is called standard phenology detection. In contrast, little effort has been devoted to real-time and short-term predictions of vegetation phenology. This is due to the lack of timely available satellite datasets and generic methods for processing noisy time series of timely available satellite observations. However, a system for real-time and short-term prediction of vegetation phenology using satellite datasets is needed to assist diverse applications, such as forecasting crop yields (Mkhabela et al. 2005; Weissteiner and Kühbauch 2005), fire danger (Roads et al. 2005), soil moisture content (White and Nemani 2004) and the timing of allergenic pollen occurrences and duration (Karlsen et al. 2008); detecting disturbance in forests related to hurricane destruction (McNulty 2002); monitoring insect pest phenology (Mussey and Potter 1997); and modeling seasonal carbon sequestration (Baldocchi et al. 2001; Churkina et al. 2005; Gray et al. 2014). Moreover, the presence of plant leaves influences land surface albedo and exerts strong control on surface radiation budgets and the partitioning of net radiation between latent and sensible heat fluxes impacting atmospheric boundary layer processes and affecting weather prediction (Chen & Dudhia, 2001; Ek et al., 2003; Raddatz & Cummine, 2003; Richardson et al., 2013; Schwartz, 1992). Thus, vegetation phenology is expected as an input in land surface models (LSM) in numerical weather prediction (NWP) models of the National Center for Environmental Prediction (NCEP) in NOAA (Ek et al. 2003; Ek, 2011).

The successful launch of the Visible Infrared Imaging Radiometer Suite (VIIRS) instrument onboard the Suomi National Polar-orbiting Partnership (Suomi NPP) Satellite on 28 October 2011 makes real-time prediction possible because NPP VIIRS is an operational satellite operated by NOAA (National Oceanic and Atmospheric Administration) and provides land surface observations in a timely fashion (Cao et al. 2013). The VIIRS instrument is a new generation of moderate-resolution imaging radiometer following the legacy of MODIS on Terra and Aqua satellites and AVHRR on NOAA satellites (Justice et al. 2013; Román et al. 2012). It was primarily designed to meet the needs of the operational weather community, but it still retains much of the MODIS capability for land science. The VIIRS data have been applied for monitoring land surface changes, such as wildfire (Schroeder et al., 2014) and land surface temperature (Liu et al., 2015). However, the application in land surface phenology detections has not been conducted except that a local study in central Iowa of the United States demonstrates the capability of the VIIRS time series to provide accurate phenology detections (Zhang et al., 2017).

During the past decade, several approaches have been proposed for near real-time prediction of vegetation growth using satellite datasets. Near real-time monitoring of vegetation health and drought impacts has been implemented by smoothing near real-time AVHRR observations (Kogan et al., 1997; Bokusheva et al, 2016) and "expedited" MODIS (eMODIS, a latency less than 24 hours) data (Brown et al., 2015). In phenology prediction, White and Nemani (2006) developed an algorithm using a specific vegetation index threshold for each phenoregion. Nemani et al. (2009) used a modeling framework integrating satellite data, microclimate mapping, and ecosystem simulation models to forecast landscape level indicators such as vegetation phenology and productivity. More recently, for the predication of phenological timing at a pixel level, a previous study (Zhang et al. 2012) combined the climatology of vegetation phenology and available satellite observations to establish a set of potential temporal trajectories during the senescence phase at a given time. These trajectories were applied to detect foliage coloration phases in real time, to predict the timing of future phenological events, and to further determine the uncertainty of predictions.

This study aims to establish a system for real-time and short-term predictions of spring phenology in North America using VIIRS data. We strived to accomplish our objectives by (i) generating climatology of LSP using MODIS data from 2001 to 2012; (ii) simulating a set of potential temporal trajectories during the greenup phase for each pixel by integrating LSP climatology and timely available VIIRS observations; (iii) applying potential trajectories to predict greenup onset, mid greenup phase and maturity onset in real time and short term ahead and analyze the uncertainty of predictions in 2014 and 2015; and (iv) evaluating the accuracy of real-time and short-term predictions by comparing with standard VIIRS detection (as a reference) and near-surface PhenoCam data.

2. Materials and Methods

This research was to establish a system to predict spring vegetation phenology in real time and short term ahead following the general methodology summarized in figure 1. Briefly, we first calculated climatological phenology (expectation and standard deviation) from historical MODIS time series to represent the range of phenological variation. After VIIRS land surface temperature exceeded a threshold determining a winter period, we then started to simulate a set of potential temporal trajectories of spring vegetation growth based on timely available VIIRS observations and climatological phenology that varied in each simulation at a given day and pixel. From each temporal trajectory, phenological events were calculated. The mean and standard deviation of phenological events from a set of temporal trajectories were used as a prediction and uncertainty of the prediction, respectively. This processing was updated every 3 days with the accumulation of VIIRS observations. The relevant details of these procedures were described below.

2.1 Generation of climatology of vegetation phenology

Climatological phenology, which is known as climatological expectation of land surface phenology and is here referred to as multiple-year mean values (MV) and standard deviation (SD), represents the potential range of vegetation growth variations (Verhegghen et al., 2014; Verger et al., 2015). The climatological phenology was used for predicting future greenness state because it has been demonstrated that climatological information could improve the stability of near real-time predictions (Jiang et al., 2010; Verger et al. 2014). To calculate LSP climatology, we first collected daily MODIS CMG (climate modeling grid) surface reflectance measurements (MOD09CMG, Collection 6.0) at a spatial resolution of 0.05 degrees (~5 km) in North America, covering the period from 2001 to 2012. Based on daily surface spectral reflectance, a two-band enhanced vegetation index (EVI2) was then calculated for each pixel from red and near infrared reflectance by removing the blue-reflectance influence on enhanced vegetation index (EVI) through an empirical relationship between red and blue reflectance (Jiang et al. 2008). EVI2 has several advantages including that it can be derived from satellite sensors without blue reflectance, reduces noise related blue band that is relatively more sensitive to atmospheric impacts, and is functionally equivalent to EVI which is less sensitive to background reflectance and remains sensitive to high-density canopy cover (Huete et al. 2002). In order to reduce the data size and computation time, 3-day EVI2 composites were generated by selecting cloud-free observations.

Subsequently, phenological metrics in a given year were detected using the standard phenology detection algorithm that employed two years of EVI2 data. Specifically, a Hybrid Piecewise Logistic Model (HPLM) was used to reconstruct EVI2 temporal trajectories at the pixel level for a given year using a two-year time series that contain preceding half year, the given year, and succeeding half year, which was able to effectively minimize noise, such as to remove the impacts of snow and cloud covers, fill in missing observations, and smooth irregular values in the EVI2 time series (Zhang 2015). Phenological transition dates during a greenup phase were detected using the rate of change in the curvature of the reconstructed EVI2 time series. Specifically, transition dates of greenup onset and maturity onset correspond to the day of year (DOY) on which the rate of change in curvature in the EVI2 time series data exhibits local maxima (Zhang et al. 2003). The minima EVI2 in the reconstructed temporal trajectory was defined as the background value for a given pixel, which represents the EVI2 without contamination by clouds and snow cover before the start of vegetation growth. Moreover, EVI2 values at the time of greenup onset and maturity onset and the maximum EVI2 value were also calculated from the reconstructed temporal trajectory. Further, the climatology of each phenology metrics, which represented mean value (MV) and standard deviation (SD), was calculated based on the retrieved phenological parameters from 2001 to 2012 at a pixel level.

Although the MODIS and VIIRS instruments are similar, vegetation index values are not exactly the same due to the differences in spectral bands (Vargas et al. 2013). Therefore, it is necessary to calibrate the climatology of MODIS background and maximum EVI2 values, and EVI2 values at greenup onset and maturity onset in order to be comparable with VIIRS EVI2. Specifically, we first reconstructed the temporal trajectories of MODIS EVI2 (from MOD09CMG Collection

6) and VIIRS EVI2 in 2014 using Hybrid Piecewise Logistic Model (HPLM) method (Zhang 2015). Subsequently, we spatially resampled MODIS EVI2 from 5km pixel to 4km pixel to be comparable to the pixel size in VIIRS prediction (see section 2.2) using a nearest neighbor method. A linear correlation between temporal 3-day composite MODIS EVI2 and VIIRS EVI2 was established for each pixel, which was further used to calibrate MODIS climatology EVI2 values. The phenological timing was assumed to be comparable between MODIS and VIIRS phenology detections.

2.2 Simulation of potential growth trajectories and prediction of phenological timing

In this study, we used VIIRS observations to predict spring phenology. VIIRS provides global moderate-resolution data every day at the local time around 13:30 PM with 22 spectral bands covering wavelengths from 0.4 to 11.8 µm. These bands include 16 moderate-resolution bands (M bands) with a spatial resolution of 750 m at nadir, five imaging resolution bands (I bands) with a 375 m spatial resolution at nadir, and one panchromatic Day Night Band with a near constant 750 m spatial resolution throughout the scan (Cao et al. 2013). We obtained NOAA VIIRS Environmental Data Record (EDR) products for phenology prediction. The NOAA NPP VIIRS program operationally produces a set of EDR products, which are distributed through NOAA's Comprehensive Large Array-data Stewardship System (CLASS; https://www.nsof.class.noaa.gov/). VIIRS data have a latency of about 3 hours in Running S-NPP Data Exploitation (NDE) system and a default latency of 6 hours in CLASS. From the EDR products, we obtained daily spectral reflectance, daily land surface temperature (LST), quality assessment (QA), and surface type (which contains dynamics of snow cover) for each VIIRS granule where pixel size varies. We then aggregated these granule data to a resolution of 0.036

degrees (~4km). In doing this, good-quality daily observations were averaged while a fill value of 32767 was assigned if more than 2/3 of original observations in a 4km grid were bad (cloudy) or filled (no observations). This product is produced at a spatial resolution of 4km in order to be spatially comparable with the NOAA vegetation health product which has been generated since 1981 (Kogan et al. 2015; Kogan 1997), to serve as inputs for the land model in the numerical weather prediction (NWP) models of the National Center for Environmental Prediction (NCEP) in NOAA (Ek et al. 2003; Ek, 2011) and to reduce the computing time for operational purpose. EVI2 was then calculated from the spectral reflectance data of red band (I1: 0.64μm) and near infrared band (I2: 0.865μm). The daily EVI2 and LST were subsequently aggregated to 3-day data by selecting cloud-free observations. If there was more than one selection within a 3-day window, the maximum EVI2 was used but the average LST was calculated.

With the accumulation of VIIRS observations from January 1, the potential EVI2 trajectories of spring vegetation growth was simulated by combining available EVI2 observations and climatological phenology (Fig. 1). This simulation of EVI2 trajectories would not commence until the following criteria were met. (1) The date was less than one month before the climatological greenup onset (P1 in Fig.2); (2) EVI2 was not contaminated by snow; (3) LST was greater than the threshold (278 K) because vegetation is assumed to be dormant during the period of LST < 278K; (4) EVI2 was larger than background values with an increase of more than 0.02 during consecutive two 3-day periods (P2 in Fig.2).

Once the initial criteria were satisfied, a set of potential EVI2 trajectories were simulated using the logistic model for a given date based on a potential EVI2 dataset (Zhang et al., 2003):

$$EVI2(t)=\frac{c}{1+e^{a+bt}}+EVI2_{BK} \quad (1)$$

where t is time in the day of year (DOY), a is a parameter that is related to the maximum vegetation growth rate and corresponding time, b is a parameter that is associated with the rate of plant leaf development, c is the amplitude of EVI2 variation, and $EVI2_{BK}$ is the background EVI2 value. Parameters of a and b are obtained by fitting the model using time series of EVI2 data.

The potential EVI2 dataset consisted of timely available VIIRS EVI2 observations and climatological EVI2 phenological parameters. For a given date, the climatological phenological parameters, which were EVI2 values at greenup onset and maturity onset, background EVI2 value, maximum EVI2 value, and the timing of greenup onset and maturity onset, were set to vary respectively within a range of mean value and standard deviation (between MV– SD and MV + SD). Specifically, the climatological EVI2 values increased by intervals of one third of the SD and the timing increased by intervals of one day in each simulation. As a result, a set of simulated EVI2 temporal trajectories (generally more than 500) were generated in each day and each pixel. For each trajectory simulated from equation 1, we estimated the timing of greenup onset, mid greenup phase and maturity onset using the curvature change rate (Zhang et al. 2003). The mid greenup phase is the middle date during a greenup phase between greenup onset and maturity onset, which represents the time of 50% of EVI2 amplitude and matches the start of growing season defined using the threshold approach (White et al., 1997). The mean value of the phenological estimates from all curves for a given day and pixel was considered to be the prediction and the standard deviation was considered as the uncertainty of the prediction. This implementation of real-time prediction was continuously carried out during the greenup phase every 3 days. We assumed that a greenup phase ended if there were at least two smaller 3-day

EVI2 values followed by the occurrence of the maximum value. Here, we defined "short-term prediction" as the prediction before the occurrence of a phenological event, while detection around the phenological occurrence (within 3 days) was defined as "real-time prediction". After the occurrence of a phenological event, this was called "near real-time prediction".

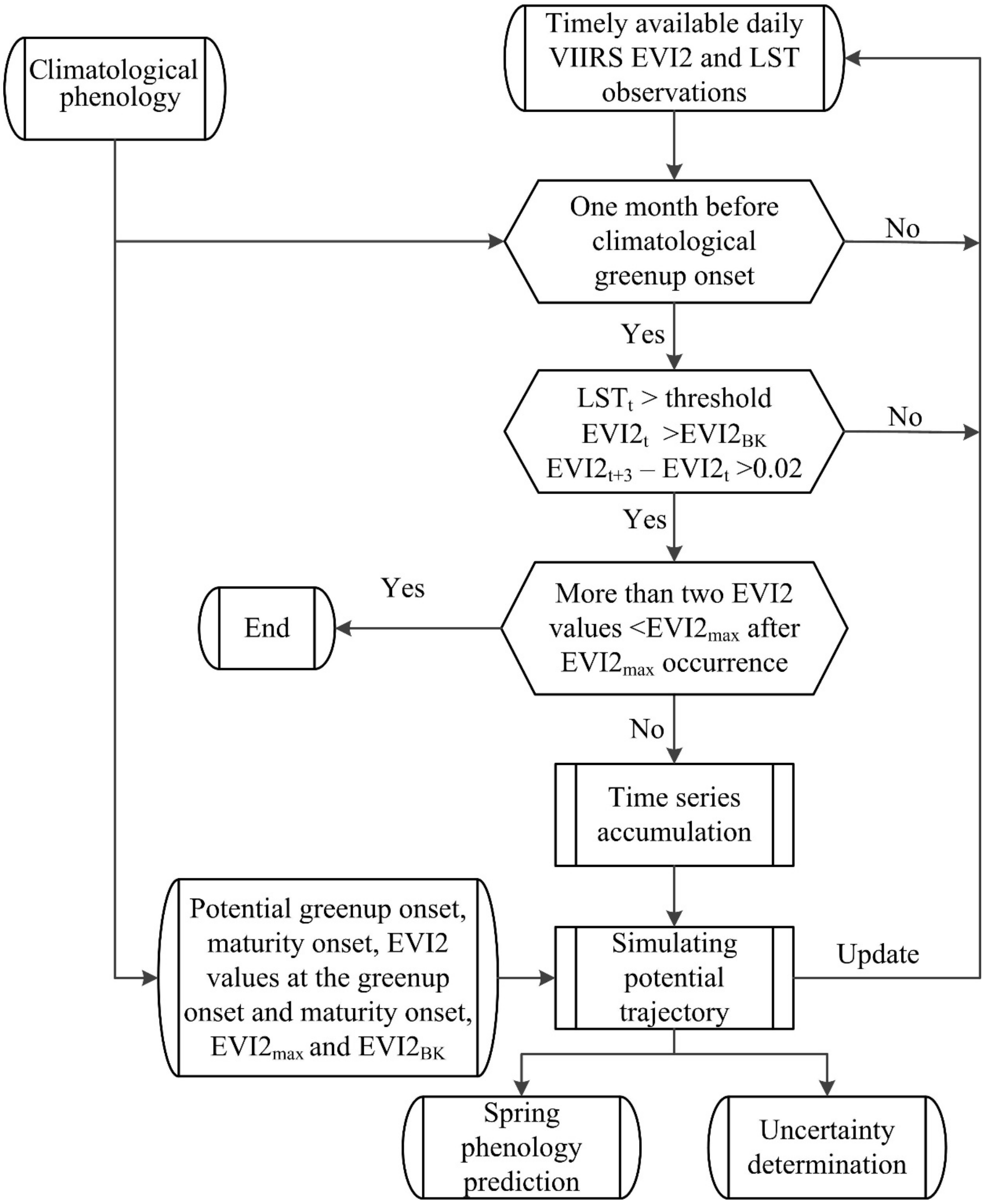

Fig.1 Flowchart of real-time and short-term predictions of spring phenology from VIIRS satellite data. The $EVI2_{max}$ represents the maximum EVI2 value during a growing season; $EVI2_{BK}$ represents background value, and LST is land surface temperature, t is the start date of simulation, t+3 is the date of EVI2 observation following start date.

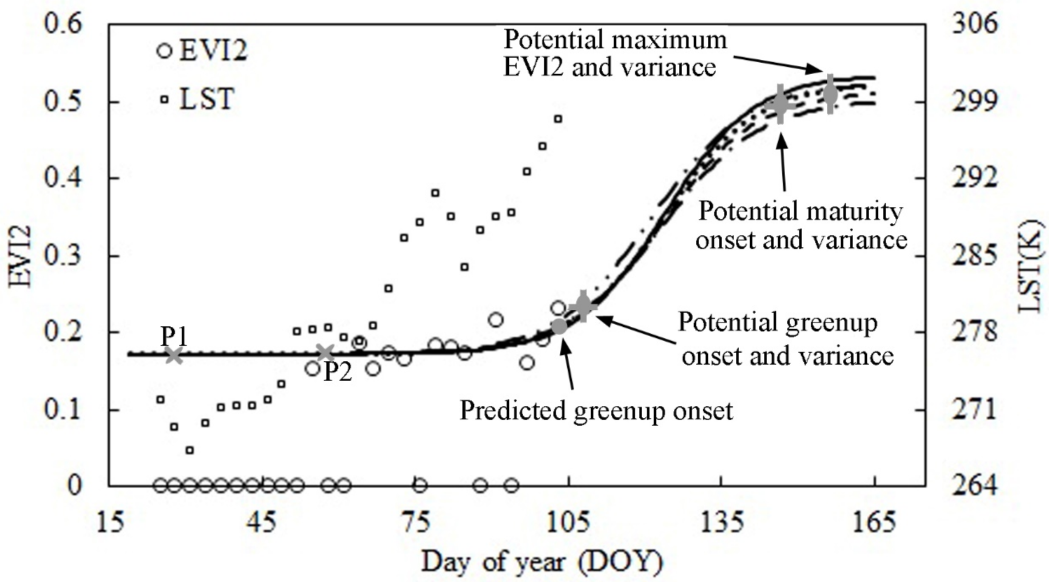

Fig.2 An example of simulating potential EVI2 temporal trajectories during a greenup phase from available EVI2 data and climatological phenology when EVI2 values at the greenup onset or maturity onset varied. The grey bar represents the potential range of timing and EVI2 values at the greenup onset and maturity onset, as well as maximum EVI2 values. The grey cross (P1) represents the date of one month before the climatological greenup onset and P2 is the start date of simulation. The EVI2 observations at the x-axis are fill values.

2.3 Assessment of real-time and short-term predictions of spring phenology

Real-time and short-term predictions of spring phenology was evaluated using three different approaches. First, the standard VIIRS detection of phenological transition dates was considered to be a reference. Specifically, the phenological metrics in 2014 and 2015 were retrieved from VIIRS EVI2 time series of July 2013-June 2015 and July 2014-June 2016, respectively, using the HPLM approach (Zhang et al., 2003, Zhang 2015). In the evaluation, we calculated the mean absolute difference (MAD) between standard detection and real-time and short-term predictions for each phenological event across North America. Second, the uncertainty in real-time and short-term predictions of phenological events was analyzed. Given that the accuracy of phenology detections could be dependent on vegetation type, MAD and uncertainty were further analyzed respectively for evergreen forest, deciduous forest, mixed forest, shrubland, savanna, grassland and cropland/natural vegetation mosaic.

Third, the accuracy of real-time prediction of spring phenology from VIIRS was evaluated using near-surface PhenoCam data. The PhenoCam uses the networked digital cameras as multi-channel imaging sensors to obtain observations repeatedly (30 minutes during daytime) across a range of ecosystem types (Richardson et al. 2011). The PhenoCam network was started in 2006 at a regional level, and now has been expanded to a continental-scale observatory (Sonnentag et al., 2012; http://klima.sr.unh.edu/). It provides digital near-ground photography containing red-green-blue (RGB) channels. In this study, we selected 95 phenocam sites that were dominated by vegetation and provided good quality observations over the entire growing season in 2014 to evaluate real-time prediction of VIIRS phenology (Fig. 3). These sites were characterized by a range of vegetation types including evergreen forest (10.6%), deciduous forest (16.5%), mixed forest (24.7%), shrublands (4.7%), savannas (9.4%), grasslands (9.4%), permanent wetlands

(1.2%), cropland/natural (7.1%), croplands (5.9%) and urban and built up (10.5%). To quantify canopy greenness from the PhenoCam images, the green chromatic coordinate (GCC), which is comparable with vegetation index derived from satellite data such as NDVI and EVI (Klosterman et al. 2014), was calculated from the average of pixel digital number in red, green and blue channels over the region of interest (Wingate et al. 2015):

$$GCC = \frac{G}{(R+G+B)} \quad (2)$$

where R is the red channel, G is the green channel and B is the blue channel.

The gaps in temporal trajectory of GCC data were filled and noises were smoothed using the Hybrid Piecewise Logistic Model (HPLM) method (Zhang 2015). Then, spring phenological events including greenup onset, date of mid greenup phase and maturity onset were extracted using the curvature change rate (Zhang et al. 2003). Finally, the timings of these PhenoCam-based phenological metrics were used to evaluate real-time prediction from VIIRS in 2014 using root mean square error (RMSE), coefficient of determination (R^2), and MAD.

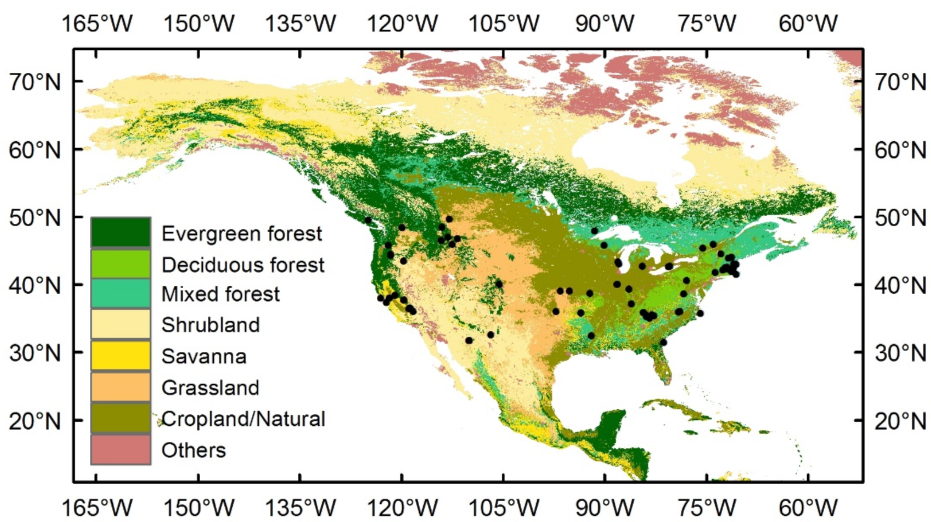

Fig.3 Spatial distribution of PhenoCam sites (solid circles) and MODIS land cover types

3 Results

3.1 Spatial pattern in real-time prediction of spring phenology

Figure 4 presents spatial patterns in real-time prediction of spring vegetation phenology across North America. Greenup onset occurred in March in southern regions, gradually shifted northwards, and reached northern areas around 50^{o}N in May and 65^{o}N in June (Fig. 4a). Relatively, greenup onset was later in most regions in 2014 than 2015 with a difference up to a month in some regions (Fig. 4a and 4d). As expected, the timing (DOY) of mid greenup phase was delayed with increasing latitudes in both years, ranging from 80 in southern areas to 200 in the northern areas (Figs.4b&4e). Maturity onset presented a similar spatial pattern, ranging from 100 at low latitudes, 140 at middle latitudes and 210 at high latitudes (Figs.4c&4f). However, spring phenology did not show a clear longitudinal pattern across North America. In mid latitudes of the United States, greenup onset was earlier in eastern region (around 75), relatively later in central region (around 90), and complex in western region (Figs.4a&4d). Moreover, phenological variation with elevation was evident. The phenological dates (DOY) were about 130 in greenup onset, 150 in mid greenup phase, and 170 in maturity onset at the top of Rocky Mountains while the corresponding dates at the base of mountains were 100-120, 120-140, 140-160, respectively. Similar pattern was also showed in Appalachia mountains. It is worth noting that a small area in central Alaska (around 63^{o}N) showed much earlier spring phenology in both 2014 and 2015 compared to similar latitudes in other areas

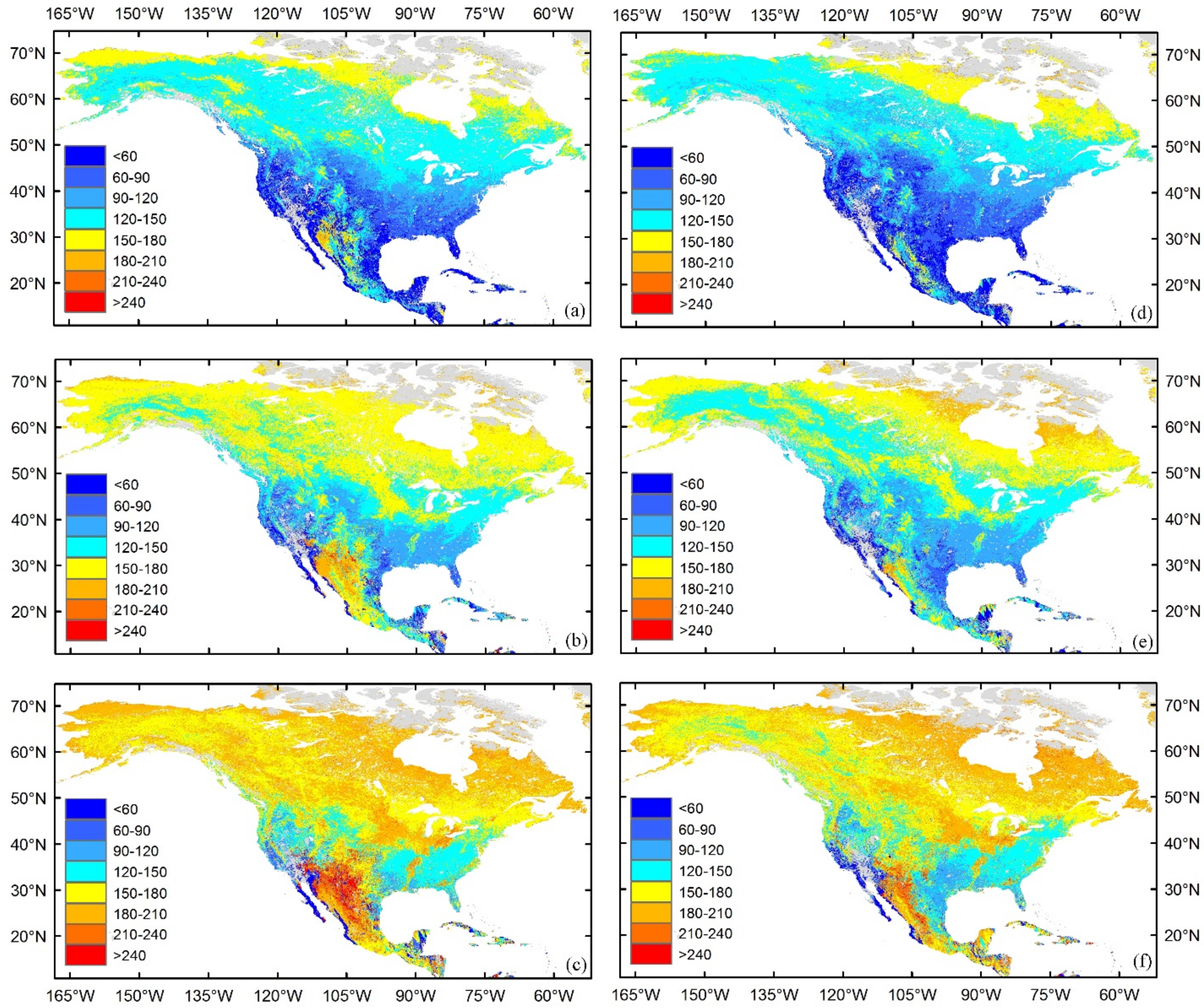

Fig.4 Spatial pattern in real-time prediction (DOY) of the onset of spring phenological events in North America in 2014 and 2015. Greenup onset (a & d), mid greenup phase (b & e) and maturity onset (c & f).

3.2 Comparison of real-time and short-term predictions with standard phenology detection

The accuracy of real-time and short-term predictions of spring phenology varied with both phenological event and the number of available VIIRS observations (Fig.5a&5c). The mean absolute difference (MAD) decreased as the number of available VIIRS EVI2 observations increased. When the prediction was carried out at about a half month prior to the phenological events in both 2014 and 2015, MAD was 15 days, 9 days and 8 days at greenup onset, mid greenup phase and maturity onset, respectively. In real time, MAD was less than 10 days for greenup onset and less than 6 days for mid greenup phase and maturity onset. Overall, MAD was relatively large for greenup onset because the available satellite observations were limited at the time of implementing prediction, whereas it was considerably decreased for mid greenup phase and maturity onset. The accuracy increased as model estimates were implemented at the time approaching the timing of the phenological events (real-time prediction).

Uncertainty in predicting spring phenology also decreased as the number of available VIIRS EVI2 observations increased (Figs.5b&5d). The uncertainty was relatively large when forecasting greenup onset and maturity onset in both 2014 and 2015, but it was smaller when forecasting mid greenup phase. Uncertainty was about 3-4 days when forecasting was undertaken in half a month earlier, and it was about 2-3 days in real-time prediction. The uncertainty was generally less than 2 days in near real-time prediction, except for maturity onset.

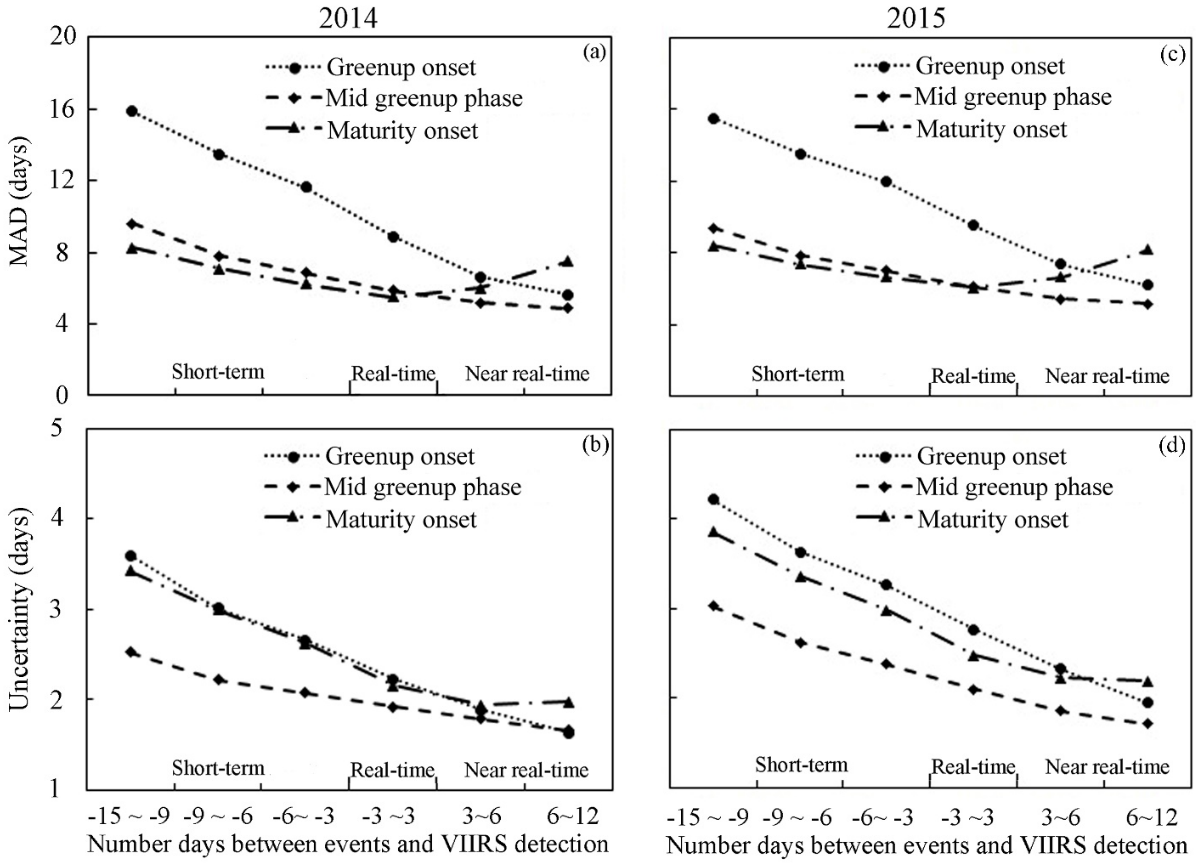

Fig.5 Mean absolute difference (a & c) and uncertainty (b & d) in real/near-real time and short-term predictions of spring phenology in North America in 2014 and 2015. The X-axis defines the different days between the date of implementing VIIRS prediction and the occurrence of phenological events derived from standard detection. Negative values represent the VIIRS detection before event occurrence (prediction in short-term ahead), while positive values indicate prediction after event occurrence (near real time prediction). The VIIRS detection carried out within 3 days before and after the event is defined as real-time prediction.

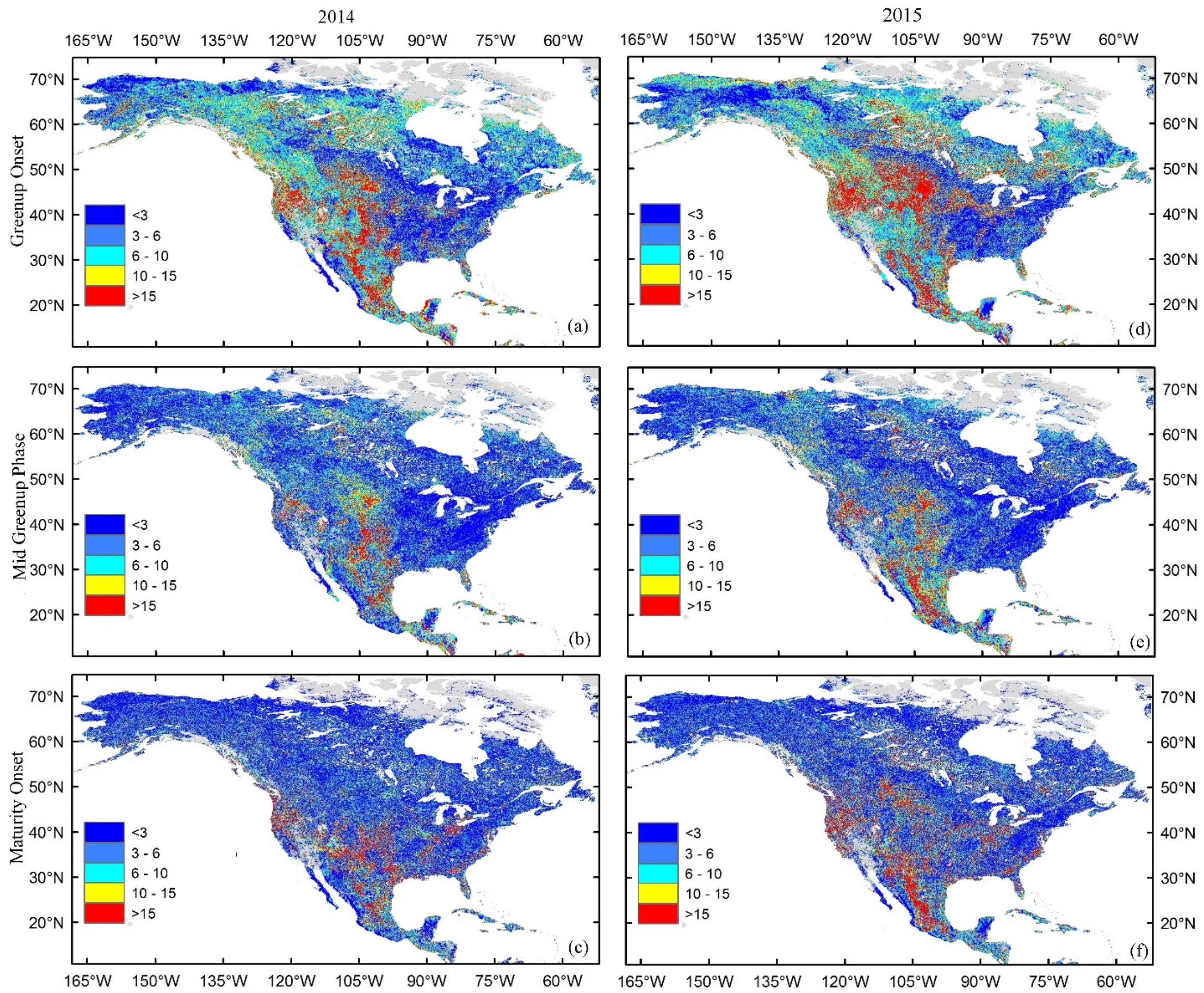

Fig.6 Spatial patterns in mean absolute difference (MAD, days) between real-time prediction of spring phenology and standard VIIRS detection in 2014 (a, b, c) and 2015 (d, e, f) . Greenup onset (a &d), mid greenup phase (b &e) and maturity onset (c & f).

Figure 6 shows spatial pattern of MAD between real-time prediction and the standard VIIRS detection. MAD for greenup onset ranged from 5 to 10 days (Fig. 6a) while it was much smaller (less than 5 days) for mid greenup phase and maturity onset in most parts of North America (Figs. 6b&6c) in 2014. A similar spatial pattern of MAD was revealed in 2015 for all three phenological events (Figs. 6d-6f). However, the MAD was relatively higher in 2015 than 2014 in the central and western United States and Mexico. In addition, MAD in the northern region for all three events was much smaller than that in the southern region for two years.

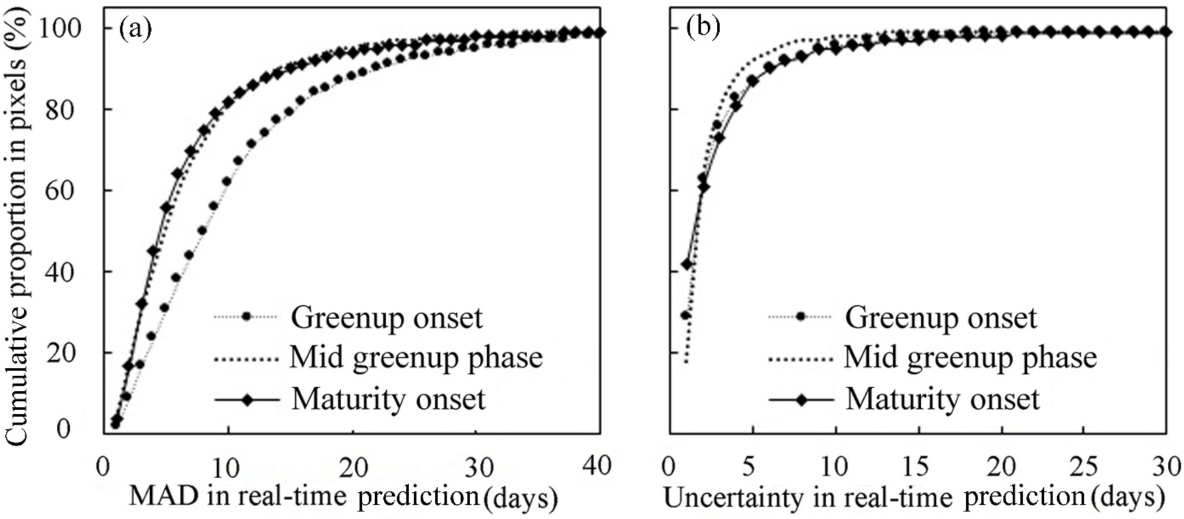

Fig.7 Pixel frequency of mean absolute difference (MAD) between real-time prediction and standard detection (a) and uncertainty in the real-time prediction (b) at various phenological events in North America in 2014.

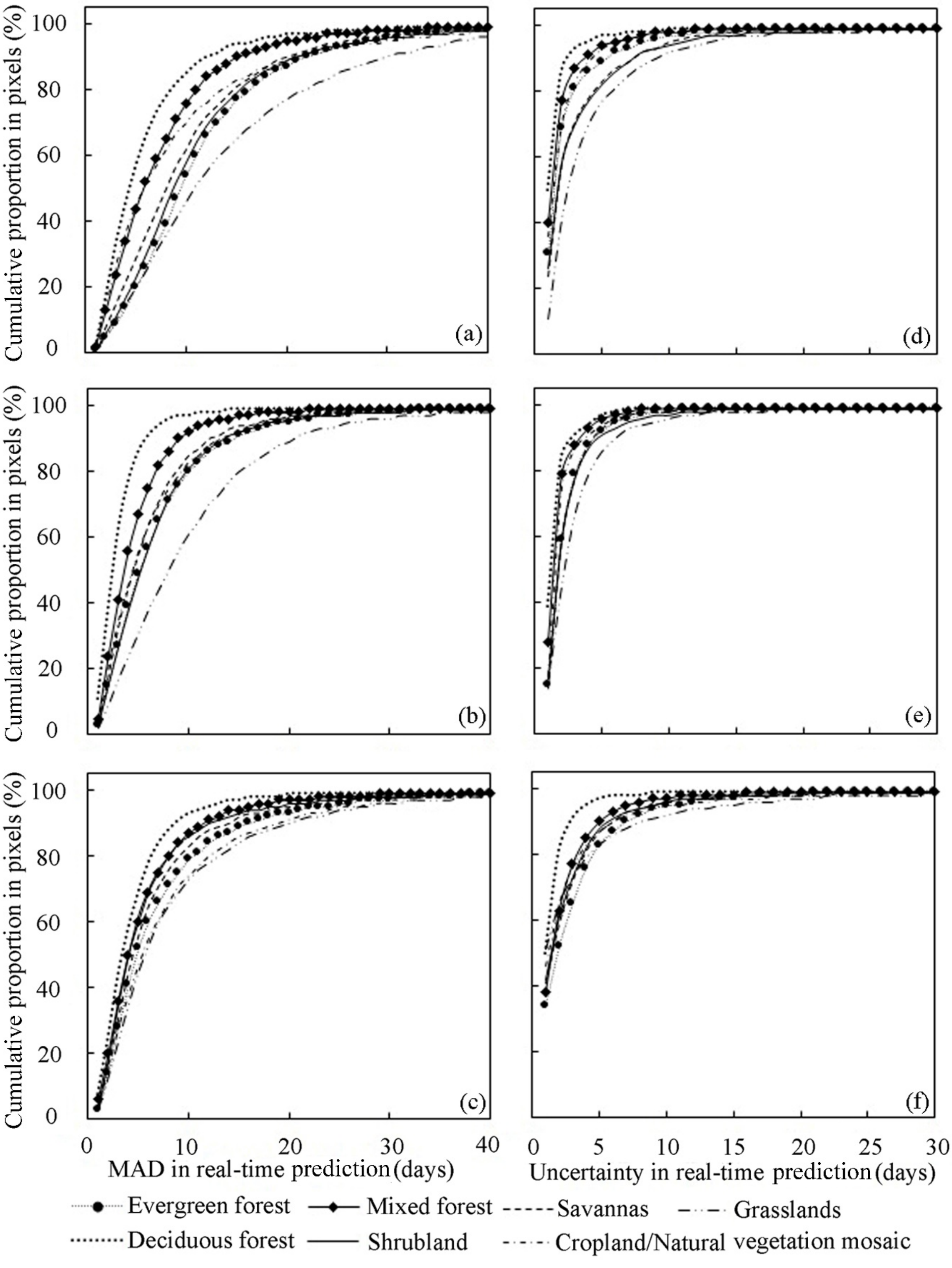
Cumulative proportion in pixels (%)
(a)
(b)
(c)
(d)
(e)
(f)
MAD in real-time prediction (days)
Uncertainty in real-time prediction (days)
Evergreen forest
Mixed forest
Savannas
Grasslands
Deciduous forest
Shrubland
Cropland/Natural vegetation mosaic

Fig.8 Pixel frequency of mean absolute difference (MAD, days) between real-time prediction and standard detection (a, b, c) and uncertainty (days) in real-time prediction of spring phenological events (d, e, f) in various ecosystem types in 2014. Greenup onset (a &d), the mid greenup phase (b &e) and maturity onset (c & f).

Overall, the pixel frequency with MAD <10 days across the North American continent was 62%, 81% and 82% in greenup onset, mid greenup phase, and maturity onset in 2014, respectively (Fig. 7a). MAD varied with land cover type across North America (Figs. 8a-8c). In real-time prediction of greenup onset, MAD was less than 10 days in 85% of deciduous forest pixels, 58% of shrubland pixels, 46% of grassland pixels and 70% of cropland/natural vegetation mosaic pixels (Fig. 8a). For the mid greenup phase, MAD was less than 5 days in 86% of deciduous forest pixels and less than 10 days in 81% of shrubland pixels, 61% of grassland pixels and 83% of cropland/natural vegetation mosaic pixels (Fig. 8b). For maturity onset, MAD was less than 7 days in 84% of deciduous forest pixels and less than 10 days in 86% of shrubland pixels, 73% of grassland pixels and 74 % of cropland/natural vegetation mosaic pixels (Fig. 8c). The MAD for each event or land cover type in 2015 was similar to 2014, which was not presented here.

Figure 9 illustrates the spatial variation in uncertainty of real-time prediction. Uncertainty was generally less than 3 days in mid-high latitudes for greenup onset, mid greenup phase and maturity onset. However, it was up to 8 days in southwestern United States and Mexico. In this area, the uncertainty in 2015 was higher than in 2014, which was likely associated with EVI2 data quality. Uncertainty also varied with spring phenological events (Fig.7b). Specifically, it was smaller for predicting the mid greenup phase than greenup onset and maturity onset. The proportion of pixels with uncertainty less than 3 days was 76%, 80% and 73% for greenup onset, mid greenup phase and maturity onset, respectively. The proportions increased to 90%, 94% and 90%, respectively, when uncertainty was less than 6 days.

The uncertainty of real-time prediction also varied across ecosystem type. Uncertainty in predicting greenup onset was less than 5 days in 97% of deciduous forest pixels, 82% of shrubland pixels and 93% of cropland/natural vegetation mosaic pixels (Fig. 8d). For real-time prediction of the mid greenup phase, it was less than 5 days in 97% of deciduous forest pixels, 91% of shrubland pixels and 94% of cropland/natural vegetation mosaic pixels (Fig. 8e). For real-time prediction of maturity onset, it was less than 5 days in 97% of deciduous forest pixels, 88% of shrubland pixels and 87% of cropland/natural vegetation mosaic pixels (Fig. 8f).

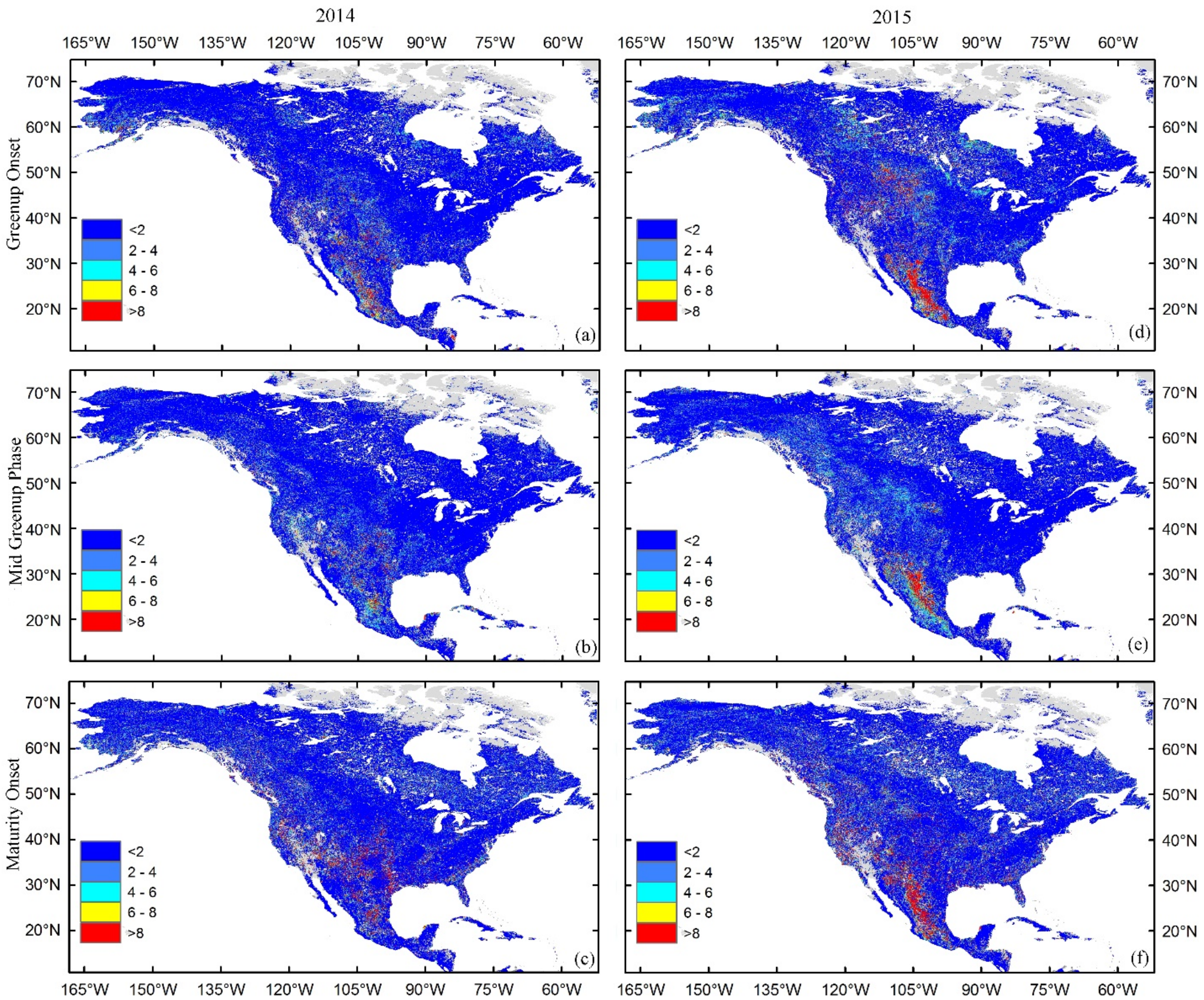

Fig.9 Spatial patterns in uncertainty (standard deviation, days) of real-time prediction of spring phenology in 2014 (a, b, c) and 2015 (d, e, f). Greenup onset (a &d), mid greenup phase (b &e) and maturity onset (c & f).

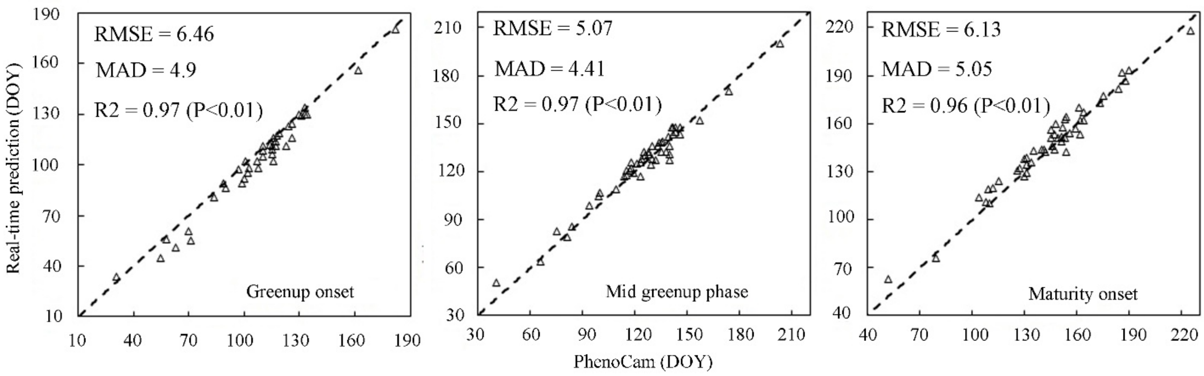

Fig.10 Comparison of spring phenological events from VIIRS real-time prediction with PhenoCam observations in 2014.

3.3 Comparison of real-time prediction of phenology with PhenoCam observations

Figure 10 shows that greenup onset, the mid greenup phase and maturity onset from real-time prediction were all significantly correlated with those derived from PhenoCam datasets ($R2 > 0.96$, $P<0.01$). The RMSE was 6.5 days, 5.1 days and 6.1 days for greenup onset, mid greenup phase and maturity onset, respectively. Correspondingly, MAD (mean absolute difference) was 4.9 days, 4.4 days and 5.1 days.

4. Discussion

The system developed in this study is robust in predicting phenological events in real time and short term ahead from near real time NPP VIIRS observations. It is expected in future to implement the real time prediction using observations from VIIRS on the Joint Polar Satellite System (JPSS) series that is planned to launch no later than March 2017 (JPSS-1) and in late 2021 (JPSS-2) (Goldberg et al. 2013). The real-time prediction system should also work well using eMODIS data (a latency of 6-10h) over the United States but the delayed release of standard MODIS observations (a latency of 6-10 days) makes real-time and short-term predictions impractical (Brown et al., 2015).

Our results show that the accuracy of real-time prediction of spring phenology is relatively higher than that in short-term prediction, which agrees well with the results in Zhang et al (2012) using MODIS dataset to predict fall foliage coloration in real time. This is expected because the contribution of climatological phenology is relatively large in short-term prediction while it gradually reduces as the number of available satellite observations increase. There are always more satellite observations available at the time in performing real-time prediction.

The mean absolute difference (MAD) between predictions and standard detections varied by phenological events. The accuracy of greenup onset predictions was lower than mid greenup phase and maturity onset predictions. This is due to the fact that a limited number of observations were available at the time of predicting vegetation greenup onset and the satellite observations were frequently contaminated by noises. Thus, the simulated potential temporal trajectories were less effective in describing vegetation development. At the time of mid greenup phase and maturity onset, more satellite observations were accumulated and the simulated temporal trajectories more closely tracked the actual vegetation growth.

Spatially, MAD in real-time prediction of spring phenology was relatively small in mid-high latitudes compared to low latitudes. This spatial pattern was mainly associated with vegetation types and climate regimes. In general, the MAD was small in deciduous forest, mixed forest and croplands that are mainly distributed in the temperate climate regime in mid-high latitudes. In this regime, vegetation growth is mostly characterized with one stable and distinctive growing cycle that is primarily driven by temperature (Liu et al., 2017; Yue et al., 2015; Schwartz et al, 2000; Zhang et al., 2004). However, the MAD was relatively large in semi-arid and arid regions of the western United States where shrublands, grasslands, and savannas are dominant. In the semi-arid and arid regions, vegetation seasonality is subtle, mainly controlled by precipitation, and varies greatly interannually (Matthews and Mazer, 2016; Zhang et al. 2010). These lead to the difficult detection of phenological metrics even using standard approach (Ganguly et al., 2010; Zhang et al., 2006). As a result, the climatology of vegetation phenology does not represent well the variation of historical vegetation growth and the EVI2 trajectories established in real-time prediction are of high uncertainties.

The phenology prediction also reveals well spatial shifts across North America. The onset of spring phenology shifted along latitude, which occurred early in south region and shifted northwards gradually. This pattern agrees well with the findings from various previous studies based on standard satellite-based phenology detections (e.g., Zhang et al, 2003; Zhu et al, 2012). Further, the onset in spring events was delayed at higher elevations, which was evident in Appalachia Mountains and Rocky Mountains. This pattern was closely related to elevations (Bacher and Jeanneret, 1994; Barry, 1992; Hopkins, 1918; Hudson Dunn and de Beurs, 2011; Liu et al., 2014). However, compared to the regular patterns of impacts from latitudes and elevations, the effects of longitude on spring phenology is more complex because phenological events are main controlled by temperature, human activity (croplands), and precipitation from eastern, central, to western United States, respectively.

Validation of real-time phenology prediction is essential but challenging because in-situ datasets that spatially match satellite footprint are rare. In this study, comparison of real-time prediction of spring phenological dates with PhenoCam datasets revealed that their correlation was strongly significant. This suggests that the developed system is robust for operational predictions of VIIRS phenology. Moreover, the close agreement highlights that PhenoCam dataset from the networked digital camera measurements offers substantial promise for validating land surface phenology (Richardson et al. 2009; Hufkens et al., 2012; Sonnentag et al., 2012). Phenocam characterizes vegetation seasonal dynamics at a landscape scale, which has great advantages over species-specific observations for validation purpose (Soudani et al., 2008; Keenan and Richardson 2015; Klosterman et al. 2014; Rodriguez-Galiano et al. 2015). With the expansion of PhenoCam network covering various ecosystems and geographical regions, the outcomes from sufficient validations could significantly help the improvement of the system for real-time phenology prediction.

It should be noted that real-time and short-term predictions of phenological development is significantly dependent on the data quality in satellite observations. Because of cloud contamination, missing observations on land surface could last consecutively for a few weeks, which greatly reduces the accuracy of phenological predictions. To improve the accuracy of real-time and short-term predictions in future work, we expect to improve our algorithms in two ways. First, the climatology of land surface phenology could be calculated from longer MODIS time series, which could represent various potential variations in vegetation growth. Second, the number of good quality satellite observations could be increased by combining observations from eMODIS and the Advanced Baseline Imager (ABI) onboard Geostationary Operational Environmental Satellite-R Series (GOES-R). GOES-R ABI is a new generation of geostationary satellite sensor containing red (500m at nadir) and near infrared (1km at nadir) spectral bands. It was launched in November 2016 (Schmit et al., 2016) and observes the United States every 5 minutes, which provides large opportunities to obtain cloud-free observations for predicting phenology development.

5.Conclusions

This study demonstrates for the first time that vegetation phenology can be predicted in real time and short-term ahead from operational VIIRS observations across various ecosystems over North America. The prediction of the developed system is implemented by combining climatology of vegetation phenology and accumulation of timely available VIIRS observations every three days. This makes significant progress in phenology detections comparing with traditional (or standard) approaches that typically use historical satellite data to detect phenology in previous years (Jonsson and Eklundh 2002; White et al. 1997; Zhang et al. 2006; Ganguly et al. 2010). More importantly, this product is expected to be employed by users for monitoring crop growth (such as United States Department of Agriculture, USDA), predicting weather conditions (such as NOAA), and observing vegetation phenology (such as USA National Phenology Network).

The accuracy of phenological prediction in this developed system increases with the accumulation of VIIRS observations and from early events to late events. Evaluations revealed that the real-time prediction of spring phenology from VIIRS data was significantly correlated with phenological metrics derived from PhenoCam. In particular, their RMSE (root mean square error) was 6 days and MAD (mean absolute difference) was less than 5 days. The comparison with standard phenology detection further showed that MAD was less than 10 days, 5 days and 5 days in greenup onset, mid greenup phase and maturity onset, respectively. MAD also varied with vegetation types. Specifically, MAD in real-time prediction of greenup onset was less than 10 days in 85% of deciduous forests while it was less than 10 days in 46% of grasslands. Finally, this system is able to produce the uncertainty in prediction, which was generally less than 3 days in mid-high latitudes for greenup onset, mid greenup phase and maturity onset although it was up to 8 days in southwestern United States and Mexico.

Acknowledgment

This work was supported by NOAA contract JPSS_PGRR2_14 and NASA contracts NNX15AB96A and NNX14AJ32G. The authors would thank Alison Donnelly for her insight on vegetation biological properties, and editing of English language and style.

References

Ault, T.R., Zurita-Milla, R., & Schwartz, M.D. (2015). A Matlab© toolbox for calculating spring indices from daily meteorological data. Computers & Geosciences, 83, 46-53

Bacher, F., & Jeanneret, F. (1994). Phenology as a tool in topoclimatology. In M. Beniston (Ed.), Mountain environments in changing climates (pp. 217–226). New York: Rutledge Press

Baldocchi, D., Falge, E., Gu, L., Olson, R., Hollinger, D., Running, S., Anthoni, P., Bernhofer, C., Davis, K., & Evans, R. (2001). FLUXNET: A new tool to study the temporal and spatial variability of ecosystem-scale carbon dioxide, water vapor, and energy flux densities. Bulletin of the American Meteorological Society, 82, 2415-2434

Barry, R. (1992). Mountain weather and climate (pp. 402). Cambridge, UK: Cambridge University Press.

Bokusheva, R., Kogan, F., Vitkovskaya, I., Conradt, S., & Batyrbayeva, M. (2016). Satellite-based vegetation health indices as a criteria for insuring against drought-related yield losses. Agricultural And Forest Meteorology, 220, 200-206

Brown, J., Howard, D., Wylie, B., Frieze, A., Ji, L., & Gacke, C. (2015). Application-Ready Expedited MODIS Data for Operational Land Surface Monitoring of Vegetation Condition. Remote Sensing, 7, 15825

Cao, C., Xiong, J., Blonski, S., Liu, Q., Uprety, S., Shao, X., Bai, Y., & Weng, F. (2013). Suomi NPP VIIRS sensor data record verification, validation, and long-term performance monitoring. Journal of Geophysical Research: Atmospheres, 118, 11, 664-11,678

Chen, F., & Dudhia, J. (2001). Coupling an Advanced Land Surface–Hydrology Model with the Penn State–NCAR MM5 Modeling System. Part I: Model Implementation and Sensitivity. Monthly Weather Review, 129, 569-585

Churkina, G., Schimel, D., Braswell, B.H., & Xiao, X. (2005). Spatial analysis of growing season length control over net ecosystem exchange. Global Change Biology, 11, 1777-1787

Cleland, E.E., Chuine, I., Menzel, A., Mooney, H.A., & Schwartz, M.D. (2007). Shifting plant phenology in response to global change. Trends in Ecology & Evolution, 22, 357-365

Ek, M. B., Mitchell, K. E., Lin, Y., Rogers, E., Grunmann, P., Koren,V., Gayno, G., & Tarpley, J. D. (2003). Implementation of Noah land surface model advances in the National Centers for Environmental Prediction operational mesoscale Eta model. Journal of Geophysical Research: Atmospheres, 108, doi:10.1029/2002JD003296

Ek, M.B. (2011). NCEP land-surface modeling. NWP workshop on model physics. Suitland, Maryland, 26-28 July 2011.

Fisher, J., & Mustard, J. (2007). Cross-scalar satellite phenology from ground, Landsat, and MODIS data. Remote Sensing of Environment, 109, 261-273

Ganguly, S., Friedl, M.A., Tan, B., Zhang, X., & Verma, M. (2010). Land surface phenology from MODIS: Characterization of the Collection 5 global land cover dynamics product. Remote Sensing of Environment, 114, 1805-1816

Goldberg, M.D., Kilcoyne, H., Cikanek, H., & Mehta, A. (2013). Joint Polar Satellite System: The United States next generation civilian polar-orbiting environmental satellite system. Journal of Geophysical Research: Atmospheres, 118, 13,463-413,475

Gray, J.M., Frolking, S., Kort, E.A., Ray, D.K., Kucharik, C.J., Ramankutty, N., & Friedl, M.A. (2014). Direct human influence on atmospheric CO2 seasonality from increased cropland productivity. Nature, 515, 398-401

Henebry, G.M., & de Beurs, K.M. (2013). Remote sensing of land surface phenology: A prospectus. In M.D. Schwartz (Ed.), Phenology: An integrative environmental science, 385-411

Hopkins, A. D. (1918). The bioclimatic law. Monthly Weather Review (Suppl. 9).

Hudson Dunn, A; de Beurs, K.M. Land surface phenology of North American mountain environments using moderate resolution imaging spectroradiometer data. Remote Sens. Environ. 2011, 115, 1220-1233.

Huete, A., Didan, K., Miura, T., Rodriguez, E.P., Gao, X., & Ferreira, L.G. (2002). Overview of the radiometric and biophysical performance of the MODIS vegetation indices. Remote Sensing of Environment, 83, 195-213

Hufkens, K., Friedl, M., Sonnentag, O., Braswell, B.H., Milliman, T., & Richardson, A.D. (2012). Linking near-surface and satellite remote sensing measurements of deciduous broadleaf forest phenology. Remote Sensing Of Environment, 117, 307-321

Jiang, B., Liang, S., Wang, J., & Xiao, Z. (2010). Modeling MODIS LAI time series using three statistical methods. Remote Sensing of Environment, 114, 1432-1444

Jiang, Z., Huete, A.R., Didan, K., & Miura, T. (2008). Development of a two-band enhanced vegetation index without a blue band. Remote Sensing of Environment, 112, 3833-3845

Jonsson, P., & Eklundh, L. (2002). Seasonality extraction by function fitting to time-series of satellite sensor data. IEEE Transactions on Geoscience and Remote Sensing, 40, 1824-1832

Justice, C.O., Román, M.O., Csiszar, I., Vermote, E.F., Wolfe, R.E., Hook, S.J., Friedl, M., Wang, Z., Schaaf, C.B., Miura, T., Tschudi, M., Riggs, G., Hall, D.K., Lyapustin, A.I., Devadiga, S., Davidson, C., & Masuoka, E.J. (2013). Land and cryosphere products from Suomi NPP VIIRS: Overview and status. Journal of Geophysical Research: Atmospheres, 118, 9753-9765

Karlsen, S.R., Ramfjord, H., Høgda, K.A., Johansen, B., Danks, F.S., & Brobakk, T.E. (2008). A satellite-based map of onset of birch (Betula) flowering in Norway. Aerobiologia, 25, 15-25

Keenan, T.F., & Richardson, A.D. (2015). The timing of autumn senescence is affected by the timing of spring phenology: implications for predictive models. Global Change Biology, 21, 2634-2641

Klosterman, S., Hufkens, K., Gray, J., Melaas, E., Sonnentag, O., Lavine, I., Mitchell, L., Norman, R., Friedl, M., & Richardson, A. (2014). Evaluating remote sensing of deciduous forest phenology at multiple spatial scales using PhenoCam imagery, Biogeosciences, 11, 4305-4320

Kogan, F., Goldberg, M., Schott, T., & Guo, W. (2015). Suomi NPP/VIIRS: improving drought watch, crop loss prediction, and food security. International Journal of Remote Sensing, 36, 5373-5383

Kogan, F.N. (1997). Global drought watch from space. Bulletin of the American Meteorological Society, 78, 621-636

Liu, L., Liu, L., Liang, L., Donnelly, A., Park, I., & Schwartz, M. (2014). Effects of elevation on spring phenological sensitivity to temperature in Tibetan Plateau grasslands. Chinese Science Bulletin, 59, 4856-4863

Liu, L., Liang, L., Schwartz, M.D., Donnelly, A., Wang, Z., Schaaf, C.B., & Liu, L. (2015). Evaluating the potential of MODIS satellite data to track temporal dynamics of autumn phenology in a temperate mixed forest. Remote Sensing of Environment, 160, 156-165

Liu, Y., Yu, Y., Yu, P., Göttsche, F., & Trigo, I. (2015). Quality Assessment of S-NPP VIIRS Land Surface Temperature Product. Remote Sensing, 7, 12215- -12241

Liu, L., Zhang, X., Yu, Y., & Donnelly, A. (2017). Detecting spatiotemporal changes of peak foliage coloration in deciduous and mixed forests across the Central and Eastern United States. Environmental Research Letters

Matthews, E.R., & Mazer, S.J. (2016). Historical changes in flowering phenology are governed by temperature × precipitation interactions in a widespread perennial herb in western North America. New Phytologist, 210, 157-167

McNulty, S.G. (2002). Hurricane impacts on US forest carbon sequestration. Environmental Pollution, 116, Supplement 1, S17-S24

Menzel, A., Sparks, T., Estrella, N., Koch, E., Aasa, A., Ahas, R., Alm-Kübler, K., Bissolli, P., Braslavská, O., & Briede, A. (2006). European phenological response to climate change matches the warming pattern. Global Change Biology, 12, 1969-1976

Mkhabela, M.S., Mkhabela, M.S., & Mashinini, N.N. (2005). Early maize yield forecasting in the four agro-ecological regions of Swaziland using NDVI data derived from NOAA's-AVHRR. Agricultural and Forest Meteorology, 129, 1-9

Moulin, S., Kergoat, L., Viovy, N., & Dedieu, G. (1997). Global-scale assessment of vegetation phenology using NOAA/AVHRR satellite measurements. Journal of Climate, 10, 1154-1170

Mussey, G.J., & Potter, D.A. (1997). Phenological Correlations Between Flowering Plants and Activity of Urban Landscape Pests in Kentucky. Journal of Economic Entomology, 90, 1615-1627

Nemani, R., Hashimoto, H., Votava, P., Melton, F., Wang, W., Michaelis, A., Mutch, L., Milesi, C., Hiatt, S., & White, M. (2009). Monitoring and forecasting ecosystem dynamics using the Terrestrial Observation and Prediction System (TOPS). Remote Sensing of Environment, 113, 1497-1509

Raddatz, R.L., & Cummine, J.D. (2003). Inter-annual Variability of Moisture Flux from the Prairie Agro-ecosystem: Impact of Crop Phenology on the Seasonal Pattern of Tornado Days. Boundary-layer Meteorology, 106, 283-295

Reed, B.C., Brown, J.F., VanderZee, D., Loveland, T.R., Merchant, J.W., & Ohlen, D.O. (1994). Measuring phenological variability from satellite imagery. Journal of Vegetation Science, 5, 703-714

Richardson, A., Friedl, M., Frolking, S., Pless, R., & Collaborators, P. (2011). PhenoCam: A continental-scale observatory for monitoring the phenology of terrestrial vegetation. In, AGU Fall Meeting Abstracts #B11D-0517

Richardson, A.D., T.F. Keenan, M. Migliavacca, O. Sonnentag, Y. Ryu, and M. Toomey. 2013. Climate change, phenology, and phenological control of vegetation feedbacks to the climate system. Agricultural and Forest Meteorology, 169: 156-173.

Richardson, A.D., Braswell, B.H., Hollinger, D.Y., Jenkins, J.P., & Ollinger, S.V. (2009). Near-surface remote sensing of spatial and temporal variation in canopy phenology. Ecological Applications, 19, 1417-1428

Roads, J., Fujioka, F., Chen, S., & Burgan, R. (2005). Seasonal fire danger forecasts for the USA. International Journal of Wildland Fire, 14, 1-18

Rodriguez-Galiano, V.F., Dash, J., & Atkinson, P.M. (2015). Intercomparison of satellite sensor land surface phenology and ground phenology in Europe. Geophysical Research Letters, 42, 2253-2260

Román, M.O., Csiszar, I., Justice, C., Key, J., Privette, J., Devadiga, S., Davidson, C., Wolfe, R.E., & Masuoka, E.J. (2012). Status of the Suomi NPP visible/infrared imager radiometer suite's (VIIRS) land environmental data records (EDRs) after early evaluation of on-orbit performance. In, 2012 IEEE International Geoscience and Remote Sensing Symposium, 1084-1087

Schmit, T.J., Griffith, P., Gunshor, M.M., Daniels, J.M., Goodman, S.J., & Lebair, W.J. (2016) A Closer Look at the ABI on the GOES-R Series. Bulletin of the American Meteorological Society, DOI: http://dx.doi.org/10.1175/BAMS-D-15-00230.1

Schroeder, W., Oliva, P., Giglio, L. and Csiszar, I. (2014). The New VIIRS 375 m Active Fire Detection Data Product: Algorithm Description and Initial Assessment. Remote Sensing of Environment, 143, 85-96

Schwartz, M.D. (1992). Phenology and Springtime Surface-Layer Change. Monthly Weather Review, 120, 2570-2578

Schwartz, M.D., Hanes, J.M., & Liang, L. (2013). Comparing carbon flux and high-resolution spring phenological measurements in a northern mixed forest. Agricultural and Forest Meteorology, 169, 136-147

Schwartz, M.D., & Reiter, B.E. (2000). Changes in North American spring. International Journal of Climatology, 20, 929-932

Sonnentag, O., Hufkens, K., Teshera-Sterne, C., Young, A.M., Friedl, M., Braswell, B.H., Milliman, T., O'Keefe, J., & Richardson, A.D. (2012). Digital repeat photography for phenological research in forest ecosystems. Agricultural And Forest Meteorology, 152, 159-177

Soudani, K., le Maire, G., Dufrêne, E., François, C., Delpierre, N., Ulrich, E., & Cecchini, S. (2008). Evaluation of the onset of green-up in temperate deciduous broadleaf forests derived from Moderate Resolution Imaging Spectroradiometer (MODIS) data. Remote Sensing Of Environment, 112, 2643-2655

Stöckli, R., & Vidale, P.L. (2004). European plant phenology and climate as seen in a 20-year AVHRR land-surface parameter dataset. International Journal of Remote Sensing, 25, 3303-3330

Vargas, M., Miura, T., Shabanov, N., & Kato, A. (2013). An initial assessment of Suomi NPP VIIRS vegetation index EDR. Journal of Geophysical Research: Atmospheres, 118, 12,301-312,316

Verger,A., Baret, F., Weiss, M., Filella, I., Peñuelas, J. (2014) Quantification of leaf area index anomalies from global VEGETATION observations, Global vegetation monitoring and modeling ((available at https://colloque.inra.fr/gv2m/Oral-Sessions). Avignon (France))

Verger, A., Baret, F., Weiss, M., Filella, I., & Peñuelas, J. (2015). GEOCLIM: A global climatology of LAI, FAPAR, and FCOVER from VEGETATION observations for 1999–2010. Remote Sensing of Environment, 166, 126-137

Verhegghen, A., Bontemps, S., & Defourny, P. (2014). A global NDVI and EVI reference data set for land-surface phenology using 13 years of daily SPOT-VEGETATION observations. International Journal of Remote Sensing, 35, 2440-2471

Weissteiner, C.J., & Kühbauch, W. (2005). Regional Yield Forecasts of Malting Barley (Hordeum vulgare L.) by NOAA-AVHRR Remote Sensing Data and Ancillary Data. Journal of Agronomy and Crop Science, 191, 308-320

White, M.A., & Nemani, R.R. (2004). Soil water forecasting in the continental United States: relative forcing by meteorology versus leaf area index and the effects of meteorological forecast errors. Canadian Journal of Remote Sensing, 30, 717-730

White, M.A., & Nemani, R.R. (2006). Real-time monitoring and short-term forecasting of land surface phenology. Remote Sensing of Environment, 104, 43-49

White, M.A., Thornton, P.E., & Running, S.W. (1997). A continental phenology model for monitoring vegetation responses to interannual climatic variability. Global Biogeochemical Cycles, 11, 217-234

Wingate, L., Ogée, J., Cremonese, E., Filippa, G., Mizunuma, T., Migliavacca, M., Moisy, C., Wilkinson, M., Moureaux, C., Wohlfahrt, G., Hammerle, A., Hörtnagl, L., Gimeno, C., Porcar-Castell, A., Galvagno, M., Nakaji, T., Morison, J., Kolle, O., Knohl, A., Kutsch, W., Kolari, P., Nikinmaa, E., Ibrom, A., Gielen, B., Eugster, W., Balzarolo, M., Papale, D., Klumpp, K., Köstner, B., Grünwald, T., Joffre, R., Ourcival, J.M., Hellstrom, M., Lindroth, A., George, C., Longdoz, B., Genty, B., Levula, J., Heinesch, B., Sprintsin, M., Yakir, D., Manise, T., Guyon, D., Ahrends, H., Plaza-Aguilar, A., Guan, J.H., & Grace, J. (2015). Interpreting canopy development and physiology using a European phenology camera network at flux sites. Biogeosciences, 12, 5995-6015

Yue, X., Unger, N., Keenan, T.F., Zhang, X., & Vogel, C.S. (2015). Probing the past 30-year phenology trend of US deciduous forests. Biogeosciences, 12, 4693-4709

Zhang, X. (2015). Reconstruction of a complete global time series of daily vegetation index trajectory from long-term AVHRR data. Remote Sensing of Environment, 156, 457-472

Zhang, X., Friedl, M.A., & Schaaf, C.B. (2006). Global vegetation phenology from moderate resolution imaging spectroradiometer (MODIS): evaluation of global patterns and comparison with in situ measurements. Journal of Geophysical Research, 111, G04017

Zhang, X., Goldberg, M.D., & Yu, Y. (2012). Prototype for monitoring and forecasting fall foliage coloration in real time from satellite data. Agricultural and Forest Meteorology, 158–159, 21-29

Zhang, X., Tan, B., & Yu, Y. (2014). Interannual variations and trends in global land surface phenology derived from enhanced vegetation index during 1982–2010. International Journal of Biometeorology, 1-18

Zhang, X.Y., Friedl, M.A., Schaaf, C.B., Strahler, A.H., Hodges, J.C.F., Gao, F., Reed, B.C., & Huete, A. (2003). Monitoring vegetation phenology using MODIS. Remote Sensing of Environment, 84, 471-475

Zhang, X., Wang, J., Gao, F., Liu, Y., Schaaf, C., Friedl, M., Yu, Y., Jayavelu, S., Gray, J., Liu, L., Yan, D., & Henebry, G.M. (2017). Exploration of scaling effects on coarse resolution land surface phenology. Remote Sensing of Environment, 190, 318-330

Zhang, X., Friedl, M.A., Schaaf, C.B., & Strahler, A.H. (2004). Climate controls on vegetation phenological patterns in northern mid-and high latitudes inferred from MODIS data. Global Change Biology, 10, 1133-1145

Zhang, X., Goldberg, M., Tarpley, D., Friedl, M., Morisette, J., Kogan, F., & Yu, Y. (2010). Drought-induced vegetation stress in southwestern North America. Environmental Research Letters, 5, 024008

Zhu, W.Q., Tian, H.Q., Xu, X.F., Pan, Y., Chen, G., & Lin, W. (2012). Extension of the growing season due to delayed autumn over mid and high latitudes in North America during 1982–2006. Global Ecology And Biogeography, 21, 260-271

LIST OF FIGURE CAPTIONS

Fig.1 Flowchart of real-time and short-term predictions of spring phenology from VIIRS satellite data. The $EVI2_{max}$ represents the maximum EVI2 value during a growing season; $EVI2_{BK}$ represents background value, and LST is land surface temperature, t is the start date of simulation, t+3 is the date of EVI2 observation following start date.

Fig.2 An example of simulating potential EVI2 temporal trajectories during a greenup phase from available EVI2 data and climatological phenology when EVI2 values at the greenup onset or maturity onset varied. The grey bar represents the potential range of timing and EVI2 values at the greenup onset and maturity onset, as well as maximum EVI2 values. The grey cross (P1) represents the date of one month before the climatological greenup onset and P2 is the start date of simulation. The EVI2 observations at the x-axis are fill values.

Fig.3 Spatial distribution of PhenoCam sites (solid circles) and MODIS land cover types

Fig.4 Spatial pattern in real-time prediction (DOY) of the onset of spring phenological events in North America in 2014 and 2015. Greenup onset (a & d), mid greenup phase (b & e) and maturity onset (c & f).

Fig.5 Mean absolute difference (a & c) and uncertainty (b & d) in real/near-real time and short-term predictions of spring phenology in North America in 2014 and 2015. The X-axis defines the different days between the date of implementing VIIRS prediction and the occurrence of phenological events derived from standard detection. Negative values represent the VIIRS detection before event occurrence (prediction in short-term ahead), while positive values indicate prediction after event occurrence (near real time prediction). The VIIRS detection carried out within 3 days before and after the event is defined as real-time prediction.

Fig.6 Spatial patterns in mean absolute difference (MAD, days) between real-time prediction of spring phenology and standard VIIRS detection in 2014 (a, b, c) and 2015 (d, e, f). Greenup onset (a &d), mid greenup phase (b &e) and maturity onset (c & f).

Fig.7 Pixel frequency of mean absolute difference (MAD) between real-time prediction and standard detection (a) and uncertainty in the real-time prediction (b) at various phenological events in North America in 2014.

Fig.8 Pixel frequency of mean absolute difference (MAD, days) between real-time prediction and standard detection (a, b, c) and uncertainty (days) in real-time prediction of spring phenological events (d, e, f) in various ecosystem types in 2014. Greenup onset (a &d), the mid greenup phase (b &e) and maturity onset (c & f).

Fig.9 Spatial patterns in uncertainty (standard deviation, days) of real-time prediction of spring phenology in 2014 (a, b, c) and 2015 (d, e, f). Greenup onset (a &d), mid greenup phase (b &e) and maturity onset (c & f).

Fig.10 Comparison of spring phenological events from VIIRS real-time prediction with PhenoCam observations in 2014.